**THE EUROPEAN
PHYSICAL JOURNAL C**

CrossMark

Photon radiation in $e^+e^- \to$ hadrons at low energies with carlomat_3.1

Fred Jegerlehner[1,2,a], **Karol Kołodziej**[3,b]

[1] Deutsches Elektronen–Synchrotron (DESY), Platanenallee 6, 15738 Zeuthen, Germany
[2] Humboldt–Universität zu Berlin, Institut für Physik, Newtonstrasse 15, 12489 Berlin, Germany
[3] Institute of Physics, University of Silesia, ul. Uniwersytecka 4, 40007 Katowice, Poland

© The Author(s) 2017. This article is an open access publication

Abstract We present a sample of results for the cross sections of several processes of low energetic e^+e^- annihilation into final states containing pions accompanied by one or two photons, or a light lepton pair. The results, which have been obtained with a new version of a multipurpose Monte Carlo program carlomat, labelled 3.1, demonstrate new capabilities of the program which, among others, include a possibility of taking into account either the initial or final state radiation separately, or both at a time, and a possibility of inclusion of the electromagnetic charged pion form factor for processes with charged pion pairs. We also discuss some problems related to the $U(1)$ electromagnetic gauge invariance.

1 Introduction

Better determination of the hadronic contribution to vacuum polarisation is indispensable to increase precision of theoretical predictions for the muon and electron $g - 2$ and to improve evolution of the fine structure constant from the Thomson limit to high energy scales. For example, $\alpha(M_Z)$ becomes particularly relevant in the context of the high energy e^+e^- collider projects [1–8], which are more and more intensively discussed in the recent years, some of them including the giga-Z option. The hadronic contribution to vacuum polarisation can be derived, with the help of dispersion relations, from the energy dependence of the ratio $R_\gamma(s) \equiv \sigma^{(0)}(e^+e^- \to \gamma^* \to \text{hadrons})/\frac{4\pi\alpha^2}{3s}$ [9,10]. For early data driven analyses, see e.g. [11,12], and for the sufficiently precise perturbative QCD results, which are needed for the perturbatively accessible windows and the high energy tail, see [13] and the references therein. Presently one is

including corrections to four loops [14]. For more recent $\alpha(M_Z)$ and $g - 2$ evaluations we refer to [15–17]. A recent update of the hadronic contribution to the electron and muon $g - 2$ [18] also accounts for the current e^+e^- data situation, as summarised below. In the regions from 5.2 to 9.46 GeV and above 13 GeV, perturbative QCD is applied. One of the main issues is $R_\gamma(s)$ in the region from 1.2 to 2.0 GeV, where more than 30 exclusive channels must be measured.

In the low energy region, which is particularly important for the dispersive evaluation of the hadronic contribution to the muon $g - 2$, data have improved dramatically in the past decade for the dominant $e^+e^- \to \pi^+\pi^-$ channel (CMD-2 [19–22], SND/Novosibirsk [23], KLOE/Frascati [24–27], BaBar/SLAC [28,29], BES-III/Beijing [30]) and the statistical errors are a minor problem now. Similarly the important region between 1.2 to 2.4 GeV has been improved a lot by the BaBar exclusive channel measurements in the ISR mode [31–46]. Recent data sets collected are: $e^+e^- \to 3(\pi^+\pi^-)$, $e^+e^- \to \bar{p}p$ and $e^+e^- \to K_S^0 K_L^0$ from CMD-3 [47–49], and $e^+e^- \to \omega\pi^0 \to \pi^0\pi^0\gamma$, $e^+e^- \to \eta\pi^+\pi^-$ and $e^+e^- \to \pi^0\gamma$ from SND [50–52]. Above 2 GeV fairly accurate BES-II data [53–55] are available. Recently, a new inclusive determination of $R_\gamma(s)$ in the range 1.84–3.72 GeV has been obtained with the KEDR detector at Novosibirsk [56,57]. However, the contribution from the range above 1 GeV is still contributing about 50% to the hadronic uncertainty of a_μ^{had}.

The main part of the hadronic uncertainty of a_μ^{had} is related to the systematic errors of the experimental data, but the uncertainties due to missing radiative corrections, which are dominated by photon radiation corrections, are quite relevant too.

To obtain reliable theoretical predictions for that many hadronic processes is a challenge indeed. It is obvious that the correct description of the most relevant hadronic channels as, e.g., $\pi^+\pi^-$, requires the inclusion of radiative cor-

[a] e-mail: fjeger@physik.hu-berlin.de

[b] e-mail: karol.kolodziej@us.edu.pl

Springer

rections. This demand is successfully met by the dedicated Monte Carlo (MC) generator PHOKHARA [58]. However, for many sub-dominant channels, with three or more particles in the final state, it is probably enough to have the leading order (LO) predictions. If those channels are measured with the method of radiative return the predictions must also include at least the initial state radiation photons. Production of hadrons at low energies, as well as the photon radiation off them, is usually described in the framework of some effective model which often includes quite a number of interaction vertices and mixing terms. Thus, it is obvious that the number of Feynman diagrams of such sub-dominant multiparticle processes may become quite big. Therefore, in order to obtain a reliable description of relatively many potentially interesting hadronic processes it is required to fully automate the process of MC code generation. This requirement has been met by version 3.0 of carlomat, a program that allows one to generate automatically the Monte Carlo programs dedicated to the description of, among others, the processes $e^+e^- \to$ hadrons at low centre-of-mass energies [59]. In addition to the standard model (SM) and some of its extensions, carlomat_3.0 includes the Feynman rules of the scalar electrodynamics (sQED), the effective vertices of electromagnetic (EM) interaction of spin 1/2 nucleons and a number of triple and quartic vertices and mixing terms resulting from the resonance chiral theory (RχT) or hidden local symmetry (HLS) model. Although there are options in the program that potentially allow one to include momentum dependence in any of the effective couplings, no such a running coupling, except for the EM form factors of the nucleons, has been actually implemented in it.

The HLS model, supplemented by isospin and SU(3) breaking effects, has been tested to work surprisingly well up to 1.05 GeV, just including the ϕ meson [60,61]. This is illustrated in the left panel of Fig. 1 for the case of the pion form factor $F_\pi(E)$.

Another important check is a comparison of the $\pi\pi$ rescattering as obtained in the model of Refs. [60,61] with data and with results once obtained by Colangelo and Leutwyler in their from first principles approach [62–65]. One of the key ingredients in this approach is the strong interaction phase shift $\delta_1^1(s)$ of $\pi\pi$ (re)scattering in the final state. We compare the phase of $F_\pi(s)$ in our model with the one obtained by solving the Roy equation with $\pi\pi$-scattering data as input. We notice that the agreement is surprisingly good up to about 1 GeV as shown in the right panel of Fig. 1.

The HLS model, which is an implementation of the vector meson dominance (VMD) model in accord with the chiral structure of QCD, includes photonic corrections treating hadrons as point-like particles. We have to address the question of the range of validity of this model. A more precise understanding of the photon radiation by hadrons is particularly important for the initial state radiation (ISR) radiative return measurements of hadronic cross sections by KLOE, BaBar and BES, which are based on sQED modelling, i.e., treating hadrons as point-like particles, of the final state radiation (FSR).

There is no doubt that sQED works at low energies if photons are relatively soft. It has been in fact utilised to account for the FSR corrections in processes involving the charged pions in the final state. Direct experimental studies of the FSR spectrum at intermediate energies, advocated e.g. in [67,68],
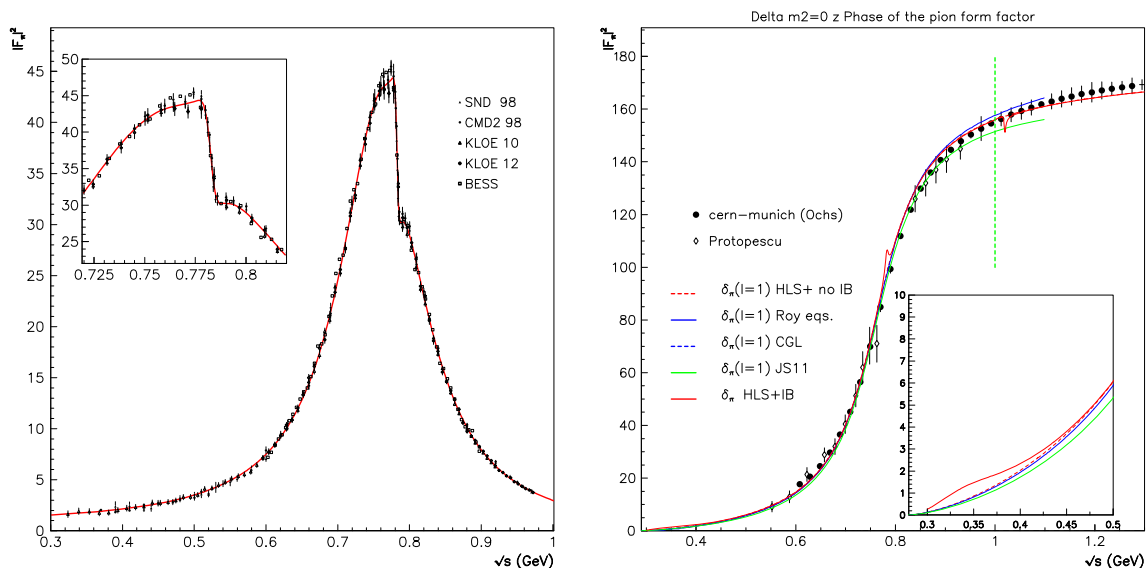

Fig. 1 The HLS model at work. The *left panel* shows the global HLS model fit of the $\pi\pi$ channel together with the data from Novosibirsk, Frascati and Beijing. The *right panel* shows the *P*-wave $\pi^+\pi^-$ phase-shift data and predictions from [62–65] and [66] together with the broken HLS phase-shift. [Reprinted with permission from Ref. [61]. Copyright (2015) by the European Physical Journal C (EPJ C)]
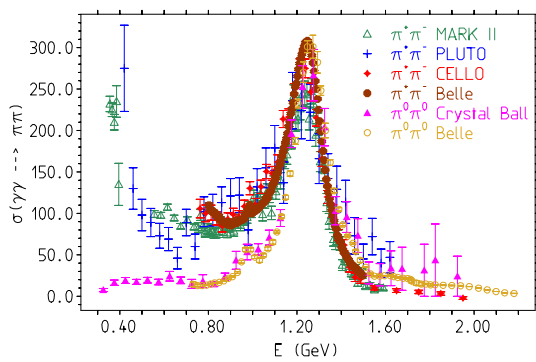
Fig. 2 How do photons couple to pions? This is obviously probed in reactions like $\gamma\gamma \to \pi^+\pi^-, \pi^0\pi^0$. One can infer from data that below about 1 GeV photons couple to pions as point-like objects (i.e. only the charged pions are produced directly). At higher energies, the photons see the quarks exclusively and form the prominent tensor resonance $f_2(1270)$. The $\pi^0\pi^0$ cross section in this figure is enhanced by the isospin symmetry factor 2, by which it is reduced in reality

are not available yet but, as far as studies exist, they seem to support sQED [69,70]. The latter, however, obviously has to break down in the hard photon regime. Here, di-pion production in $\gamma\gamma$ fusion is able to shed more light on that problem. Di-pion production cross sections are available from Crystal Ball, Mark II, JADE, PLUTO, CELLO and Belle [71–80]. We see in Fig. 2 that the $\pi^+\pi^-$ cross section is large while the $\pi^0\pi^0$ one is tiny at threshold, which means that, as expected, photons see the pions and they do not see the composite structure as they are not hard enough. The $\pi^0\pi^0$ final state is then available via strong rescattering only.

As energy of the $\pi\pi$ system increases, the strong tensor meson resonance $f_2(1270)$ shows up in both the charged and the neutral channels. Rates only differ by the isospin weight factor 2. Apparently now photons directly probe the quarks. Figure 2 also illustrates that utilising isospin relations to evaluate missing contributions to $a_\mu^{\mathrm{had,LO}}$ from unseen channels may be rather misleading, since we are dealing with hadron production mediated by one photon exchange and electromagnetic interaction obviously can violate isospin by close to 100%.

In the present work, we present a sample of results for the cross sections of several processes of low energetic e^+e^- annihilation into final states containing pions accompanied by one or two photons, or a light lepton pair. The results, which have been obtained with a new version of a multipurpose Monte Carlo program `carlomat`, labelled 3.1 [81], demonstrate new capabilities of the program. They include a possibility of taking into account either the initial or final state radiation separately, or both at a time, and a possibility of inclusion of the electromagnetic charged pion form factor for processes with charged pion pairs. We also discuss some problems related to the $U(1)$ electromagnetic gauge invariance.
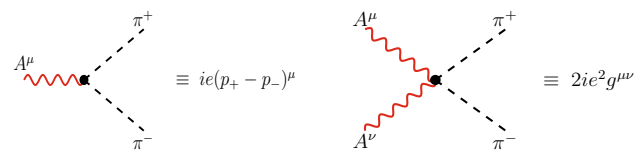

Fig. 3 Vertices of sQED

2 Theoretical framework

The production of charged pion pairs in the e^+e^- annihilation at low energies can be effectively described in the framework of scalar quantum electrodynamics (sQED), with the $U(1)$ gauge invariant Lagrangian given by

$$\mathcal{L}_\pi^{\mathrm{sQED}} = \partial_\mu\varphi \left(\partial^\mu\varphi\right)^* - m_\pi^2 \varphi\varphi^* - ie\left(\varphi^*\partial_\mu\varphi - \varphi\partial_\mu\varphi^*\right) A^\mu \\ + e^2 g_{\mu\nu}\varphi\varphi^* A^\mu A^\nu, \tag{1}$$

where $\pi^\pm$ are represented by a complex scalar field φ and the remaining notation is obvious. The interaction vertices following from the Lagrangian (1) are shown in Fig. 3.

The bound state nature of the charged pion can be taken into account by introducing in a proper way the charged pion form factor $F_\pi(q^2)$ in the Feynman rules of Fig. 3. In the time-like region, $q^2 = s > 4m_\pi^2$, the form factor is given by

$$|F_\pi(s)|^2 = \frac{\sigma^{(0)}(e^+e^- \to \gamma^* \to \pi^+\pi^-)}{\frac{\pi\alpha^2}{3s}\beta_\pi^3}$$

$$\text{with} \quad \beta_\pi = \left(1 - \frac{4m_\pi^2}{s}\right)^{\frac{1}{2}}. \tag{2}$$

Actually, the HLS model predicts the pion form factor, but one has to include one-loop self-energy corrections in order to account for the dynamically generated width of the ρ meson and its energy dependence. A separate subroutine for the form factor $F_\pi(s)$, based on a fit to data from Novosibirsk [19–23], Frascati (KLOE) [24–27], SLAC (BaBar) [28,29] and Beijing (BESIII) [30], has been written by one of us (FJ). It has been then implemented in `carlomat` by the substitution:

$$e \to eF_\pi(q^2) \tag{3}$$

in the triple coupling of Fig. 3 and appropriate modification of the quartic coupling of Fig. 3, which will be discussed later. Correctness of the implementation is cross checked by comparing the values of the form factor calculated by a direct call to the subroutine for $F_\pi(s)$ against corresponding values calculated according to Eq. (2), i.e., with the MC program for $\sigma^{(0)}(e^+e^- \to \gamma^* \to \pi^+\pi^-)$ generated automatically with `carlomat_3.1`. The results of the cross check are plotted in Fig. 4.

As the fit formula for $F_\pi(s)$ includes contributions of the virtual photon mixing with $\rho^0, \omega, \phi, \rho(1450)$ and $\rho(1700)$
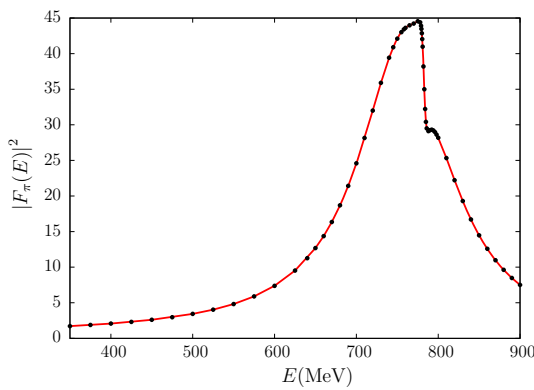
Fig. 4 The EM charged pion form factor calculated by direct calls to the subroutine for $F_\pi(s)$ (*points*) and with the MC program generated automatically (*solid line*)

vector mesons, each subsequently decaying into the $\pi^+\pi^-$-pair, substitution (3) is not justified if a real photon is radiated off the final state pion. In this case, it seems better to keep the triple coupling of Fig. 3 unchanged. However, then a question arises, how the form factor should be taken into account in the quartic coupling of Fig. 3 in order not to violate the $U(1)$ gauge invariance. To address the question let us consider the FSR in the process

$$e^+e^- \to \pi^+\pi^-\gamma \tag{4}$$

the LO Feynman diagrams of which are shown in Fig. 5, where the particle four momenta relevant for the Feynman rules of Fig. 3 have been indicated in parentheses.

Using the substitutions: (3) in the triple and $e^2 \to e^2 G_\pi(q^2)$ in the quartic vertex of Fig. 3, we get the following expressions for the amplitudes of the LO Feynman diagrams of Fig. 5:
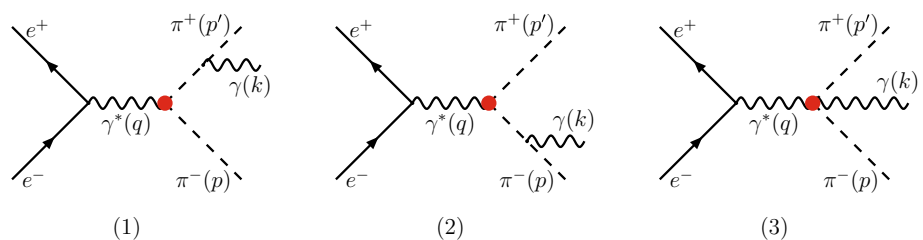
$$M_1 = j_\mu e F_\pi(q^2)(p'+k-p)^\mu \, e \, \frac{(-p'-(p'+k)) \cdot \varepsilon(k)}{(p'+k)^2 - m_\pi^2}, \tag{5}$$

$$M_2 = j_\mu e F_\pi(q^2)(p'-p-k)^\mu \, e \, \frac{((p+k)+p) \cdot \varepsilon(k)}{(p+k)^2 - m_\pi^2}, \tag{6}$$

$$M_3 = j_\mu 2e^2 G_\pi(q^2) g^{\mu\nu} \varepsilon_\nu(k), \tag{7}$$

where j stands for the initial state current contracted with the photon propagator and we have suppressed polarisation

indices both in j and in the photon polarisation four vector $\varepsilon(k)$. Now, in order to test the $U(1)$ gauge invariance, let us substitute $\varepsilon(k) \to k$ in the full FSR amplitude

$$
\begin{aligned}
M_{\mathrm{FSR}}|_{\varepsilon(k)\to k} &= (M_1 + M_2 + M_3)|_{\varepsilon(k)\to k} \\
&= j_\mu e^2 \Bigg[(p'+k-p)^\mu F_\pi(q^2) \frac{-2p' \cdot k}{2p' \cdot k} \\
&\quad + (p'-p-k)^\mu F_\pi(q^2) \frac{2p \cdot k}{2p \cdot k} + 2k^\mu G_\pi(q^2) \Bigg] \\
&= j_\mu e^2 \left[-2k^\mu F_\pi(q^2) + 2k^\mu G_\pi(q^2) \right].
\end{aligned}
\tag{8}
$$

It is obvious that the right hand side of Eq. (8) vanishes only if $G_\pi(q^2) \equiv F_\pi(q^2)$. Thus, the EM charged pion form factor should be included in the quartic vertex of Fig. 3 by the following substitutions:

$$e^2 \to e^2 F_\pi(q^2), \quad e^2 \to e^2 \left| F_\pi(q^2) \right|^2, \tag{9}$$

if one, or none, respectively, of the photon lines is on mass shell. Both possibilities of modification of e^2 are included in the program at the stage of code generation and can be controlled in the MC computation part of the program. However, the situation, where both photons in the vertex are off-shell, may lead to some ambiguity of the choice of the momentum transfer in the form factor. This is illustrated in Fig. 6, where two initial state radiation (ISR) Feynman diagrams of the process

$$e^+e^- \to \pi^+\pi^-\mu^+\mu^-\gamma \tag{10}$$

are shown. It is not at all clear, which four momentum, q or q', should be used in the charged pion form factor that is to be substituted in the quartic sQED vertex indicated by the blob. The non-trivial pion form factor is due to the VMD dressing of the photon via ρ–γ mixing, and in fact the HLS model
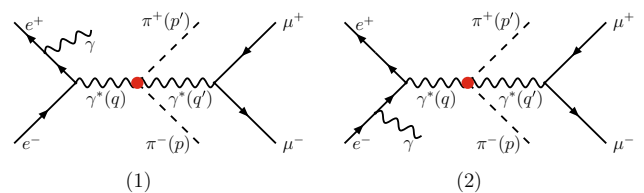

Fig. 6 ISR Feynman diagrams of process (10) in which the choice of four momentum transfer in the charged pion form factor, represented by the *red blob*, may be ambiguous

Fig. 5 FSR Feynman diagrams of process (4) in the LO. The relevant four momenta are indicated in *parentheses* and *blobs* represent the charged pion form factor

exhibits a $\rho^0\rho^0\pi^+\pi^-$ coupling as well. Thus both off-shell photons are dressed with a form factor. As q^2 is tuned to scan the ρ resonance the corresponding form factor is crucial as it exhibits large deviations from unity in the resonance region, while q'^2 is closer to the photon mass shell such that the form factor is much less important as we expect to see only the low energy tail of the resonance. A full HLS model calculation is expected to remove any ambiguity here.

However, in `carlomat_3.1`, the choice of four momentum in the form factor is made automatically and it need not be consistent between same vertices appearing in different Feynman diagrams. Such inconsistencies may lead to violation of the $U(1)$ gauge invariance. The inconsistency may also occur if we want to treat the ISR in process (10) in an inclusive way according to Eq. (1) of ref. [82], where the cross section of non-radiative process

$$e^+e^- \to \pi^+\pi^-\mu^+\mu^- \tag{11}$$

should be folded with the corresponding radiation function describing the ISR. Again, it may happen that the pion form factor in the Feynman diagram of process (11), which can be obtained either from diagram (1) or (2) of Fig. 6 by cancelling the external photon line, will be parameterised in terms of different four momenta relative to the corresponding form factor in process (10). Needless to say, such ambiguities in the choice of four momenta in the form factor may lead to substantial discrepancies between the corresponding cross sections. Therefore, it is better to use a fixed coupling in such cases.

In order to describe the processes of pion production in e^+e^- annihilation at low energies, we will use, in addition to the SM and sQED vertices of Fig. 3, if appropriate with substitutions (3) and (9), the photon–vector meson mixing of Fig. 7 and the triple and quartic vertices of the HLS model depicted, respectively, in Figs. 8 and 9.

In Figs. 7 and 8a, ρ_1 and ρ_2 stand for $\rho(1450)$ and $\rho(1700)$, respectively. If we include the EM charged pion form factor, then we neglect the contributions of the $\gamma-V$ mixing and the subsequent decay of the corresponding vector meson into $\pi^+\pi^-$-pairs, represented by the interaction vertex of Fig. 8a, as well as the contribution of the quartic vertex of Fig. 9c, as they are already included in the form factor.

3 Results

In this section, we show a sample of results for the cross sections of several processes of $e^+e^- \to$ hadrons, with the final state containing pions accompanied by one or two photons, or a light lepton pair, at $\sqrt{s} = 0.8$ GeV, $\sqrt{s} = 1.0$ GeV and $\sqrt{s} = 1.5$ GeV. The necessary MC programs have been generated taking into account the Feynman rules described in Sect. 2 and computed with the same physical input parameters as those specified in module `inprfms` of `carlomat_3.1` which is available on the web page [81]. The following cuts on the photon energy E_γ and photon angle with respect to the beam $\theta_{\gamma b}$ are imposed:

$$E_\gamma > 0.01 \text{ GeV}, \quad 5° < \theta_{\gamma b} < 175°. \tag{12}$$

$$A^\mu(q) \quad V^\nu(q) \quad \equiv -e f_{AV}(q^2)\, g^{\mu\nu}, \quad V = \rho^0, \omega, \phi, \rho_1, \rho_2$$

Fig. 7 The $\gamma-V$-mixing terms considered in the present work; ρ_1 and ρ_2 stand for $\rho(1450)$ and $\rho(1700)$, respectively

$$V^\mu(q) \quad \pi^+(p_1) \quad \pi^-(p_2) \quad \equiv i f_{V\pi^+\pi^-}(q^2)(p_1 - p_2)^\mu, \quad V = \rho^0, \omega, \phi, \rho_1, \rho_2$$

(a)

$$\pi^0(q) \quad \omega^\mu(p_1) \quad \rho^{0\nu}(p_2) \quad \equiv f_{\pi^0\omega\rho^0}(q^2)\varepsilon^{\mu\nu\alpha\beta}p_{1\alpha}p_{2\beta}$$

(b)

$$\pi^0(q) \quad A^\mu(p_1) \quad A^\nu(p_2) \quad \equiv e^2 f_{\pi^0 AA}(q^2)\varepsilon^{\mu\nu\alpha\beta}p_{1\alpha}p_{2\beta}$$

(c)

$$\pi^0(q) \quad A^\mu(p_1) \quad V^\nu(p_2) \quad \equiv i e f_{\pi^0 AV}(q^2)\varepsilon^{\mu\nu\alpha\beta}p_{1\alpha}p_{2\beta} \quad V = \rho^0, \omega$$

(d)
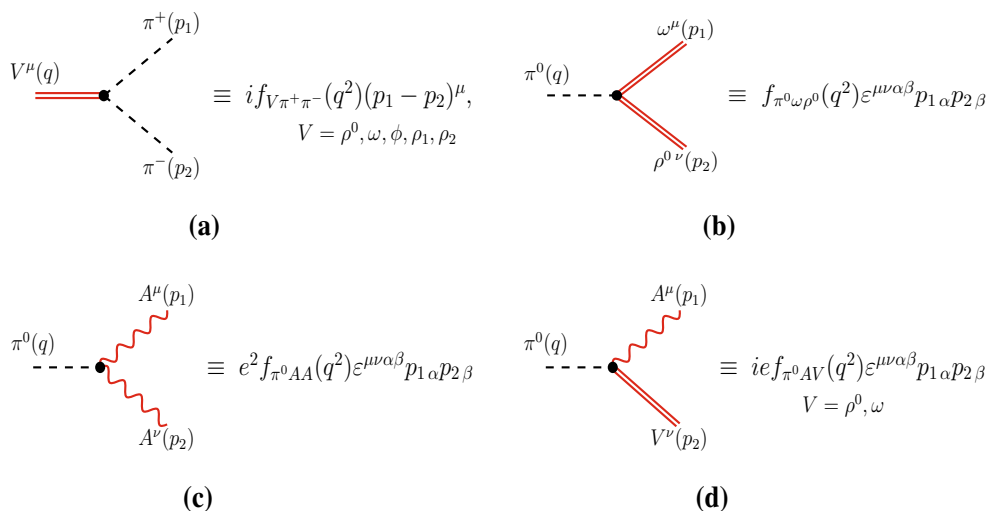
Fig. 8 Triple vertices of the HLS relevant for the present work

(a)

$$\equiv -ef_{A\pi^0\pi^+\pi^-}(q^2)\varepsilon^{\mu\nu\alpha\beta}p_{1\nu}p_{2\alpha}p_{3\beta}$$

(b)

$$\equiv -ef_{\omega\pi\pi\pi}(q^2)\varepsilon^{\mu\nu\alpha\beta}p_{1\nu}p_{2\alpha}p_{3\beta}$$

(c)

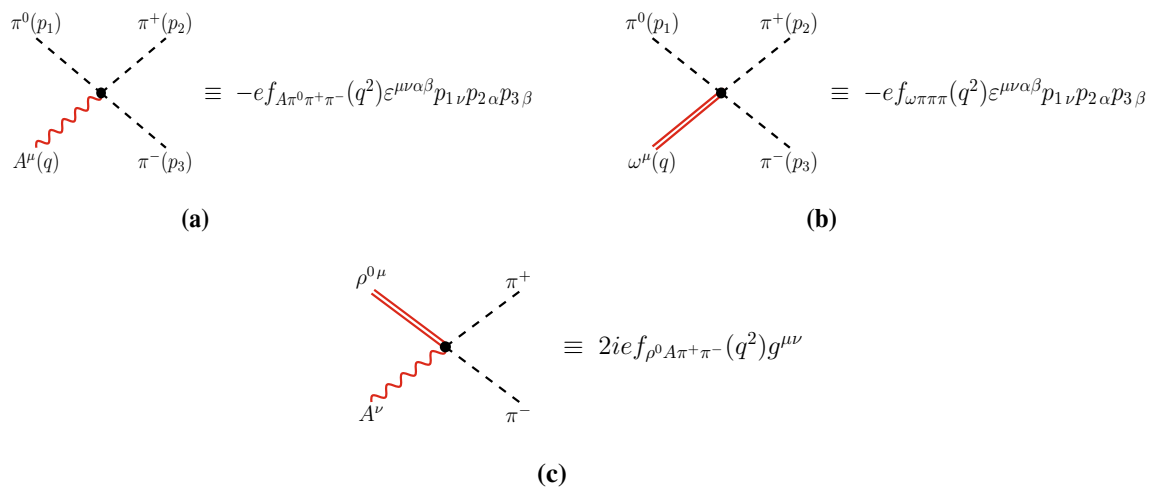$$\equiv 2ief_{\rho^0 A\pi^+\pi^-}(q^2)g^{\mu\nu}$$

Fig. 9 Quartic vertices of the HLS model taken into account in the present work

Table 1 The cross sections in pb at $\sqrt{s} = 1$ GeV and the corresponding $U(1)$ gauge invariance tests. The numbers in parentheses show the MC uncertainty of the last decimals

Process	ISR			Full LO		
$e^+e^- \to$	# diags	σ	$\sigma\|_{\varepsilon(k)=k}$	# diags	σ	$\sigma\|_{\varepsilon(k)=k}$
$\pi^+\pi^-\gamma$	2	2.041(4)e+4	1.04(1)e−28	5	2.249(4)e+4	2.73(2)e−28
$\pi^+\pi^-\pi^0\gamma$	32	409(1)	2.21(3)e−30	156	481.5(6)	3.011(1)e−2
$\pi^+\pi^-\mu^+\mu^-\gamma$	26	4.344(9)e−2	4.62(5)e−34	107	6.449(8)e−2	6.42(5)e−34
$\pi^+\pi^-\pi^+\pi^-\gamma$	36	2.029(5)e−3	2.14(3)e−35	200	3.320(5)e−3	3.03(2)e−35
$\pi^+\pi^-\gamma\gamma$	6	1.445(14)e+3	1.22(4)e−29	44	2.131(8)e+3	2.08(3)e−29
$\pi^+\pi^-\mu^+\mu^-\gamma\gamma$	90	1.127(7)e−3	1.16(4)e−35	1272	2.535(8)e−3	9.56(1)e−19
$\pi^+\pi^-\pi^+\pi^-\gamma\gamma$	120	4.68(3)e−5	4.6(1)e−37	2772	1.303(4)e−4	4.969(4)e−15

In addition to processes (4) and (10), we consider the following radiative processes with one photon:

$$e^+e^- \to \pi^+\pi^-\pi^0\gamma, \tag{13}$$
$$e^+e^- \to \pi^+\pi^-\pi^+\pi^-\gamma \tag{14}$$

and two photons:

$$e^+e^- \to \pi^+\pi^-\gamma\gamma, \tag{15}$$
$$e^+e^- \to \pi^+\pi^-\mu^+\mu^-\gamma\gamma, \tag{16}$$
$$e^+e^- \to \pi^+\pi^-\pi^+\pi^-\gamma\gamma. \tag{17}$$

The cross sections of processes (4), (10) and (13)–(17) at $\sqrt{s} = 1$ GeV, computed with cuts (12), are listed in Table 1, where each row includes the ISR and full LO total cross sections together with results of the $U(1)$ gauge invariance tests, i.e. the corresponding cross sections computed with the photon polarisation four vector $\varepsilon(k)$ replaced with its four momentum k. The replacement is made just for one photon for processes (15), (16) with two photons. For testing purposes, we also give corresponding numbers of the Feynman diagrams which `carlomat_3.1` generated for each of the

considered processes within the model with the EM charged pion form factor, except for process (13) where we give the number of diagrams generated within the HLS model with fixed couplings, as specified in Sect. 2. The gauge invariant test is satisfied perfectly well for all the ISR cross sections presented and full LO cross sections of processes (4), (10), (14) and (15), for which we observe a drop of about 32 orders of magnitude, in accordance to what can be expected with the double precision Fortran arithmetic. A less satisfactory drop of the full LO cross section of processes (16) and (17) is due to the ambiguity of the momentum transfer choice in the pion form factor $F_\pi(q^2)$ in the Feynman diagrams containing the quartic vertex of sQED with both photon lines being virtual, as discussed in Sect. 2. However, the four momentum transfer choice ambiguity cannot explain a much less satisfactory drop in the full LO cross section of process (13), presented in the second row of Table 1, where the problem is caused among others by the two Feynman diagrams shown in Fig. 10. Apparently the Feynman rules listed in Figs. 7, 8 and 9 are incomplete and there should be an extra Feynman diagram with the external photon attached to the quartic $\pi^+\pi^-\pi^0\gamma$
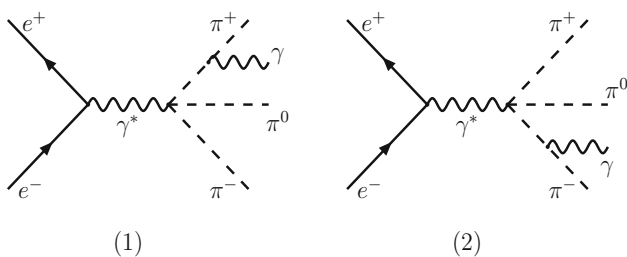
Fig. 10 The Feynman diagrams of process (13) that cause the $U(1)$ gauge invariance violation

vertex, i.e. a penta vertex, which would have cured the problem if the penta coupling had been chosen properly. Unfortunately, an inclusion of that kind of coupling is not possible in the automatic code generation, as the Feynman diagram topology generator of `carlomat` [83] includes only triple and quartic interaction vertices. However, it should be noted that the $U(1)$ gauge invariance violation concerns only the FSR part which is substantially smaller than the ISR part of the cross section. Thus, we expect that the prediction for the cross section of (13) can be still considered as being quite reliable.

It should be stressed here that `carlomat_3.1` offers a possibility to compute cross sections of other processes, e.g., with higher pion multiplicities, with neutral pions, or with charged or neutral kaons, for which a similar kind of analyses could easily be repeated.

The differential cross sections of process (4) at $\sqrt{s} = 0.8$ GeV, $\sqrt{s} = 1$ GeV and $\sqrt{s} = 1.5$ GeV are plotted in Fig. 11 as functions of the invariant mass of the $\pi^+\pi^-$-pair. In all three panels, the solid lines show the ISR cross section calculated with the MC program and the grey shaded histograms show the same cross section calculated with the corresponding analytic formula for $d\sigma_{ISR}/dQ^2$ given by Eq. (1) of Ref. [82]. As can be seen in all the three panels, the two differential cross sections agree perfectly well and small differences in a few bins of Q^2 are most probably due to statistical fluctuations, as the corresponding total cross sections agree within one standard deviation of the MC integration. The dashed lines show the full LO differential cross sections. Thus, the difference between the dashed and solid lines illustrates the FSR effect.

In order to illustrate the effect of the charged pion form factor, we compare in Fig. 12 the full LO differential cross sections of process (4), as plotted with the solid lines in Fig. 11,
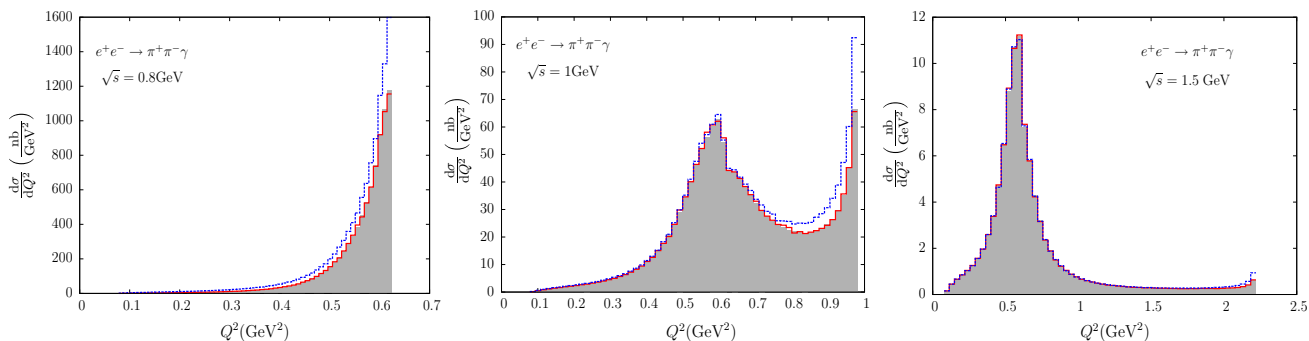

Fig. 11 The differential cross sections of process (4) as functions of invariant mass of the $\pi^+\pi^-$-pair. *The solid line* and the *shaded histogram* represent the ISR cross section, obtained with the MC program and with the analytic formula of Ref. [82], respectively, and the *dashed line* represents the full LO result. The difference between *solid* and *dashed lines* represents the FSR correction
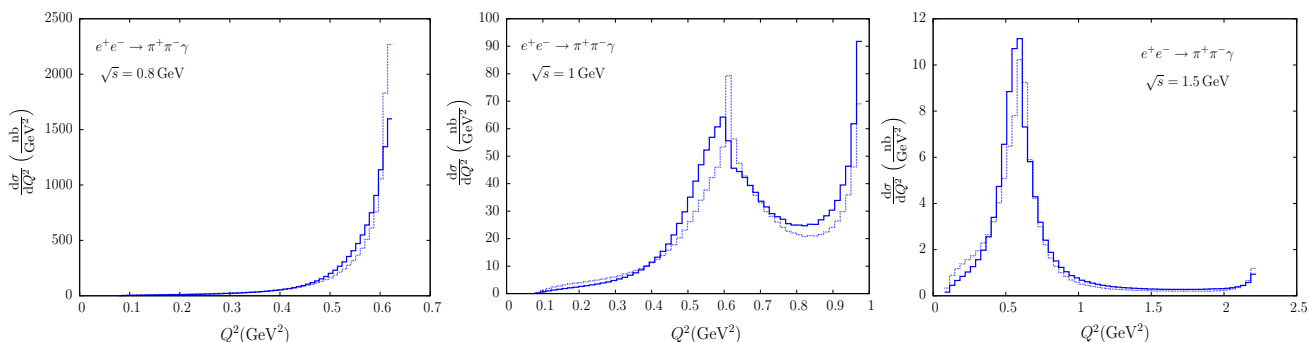

Fig. 12 The differential cross sections of (4) as functions of invariant mass of the $\pi^+\pi^-$-pair computed in a model with the charged pion form factor (*solid lines*) and in the HLS model with fixed couplings (*dotted lines*)
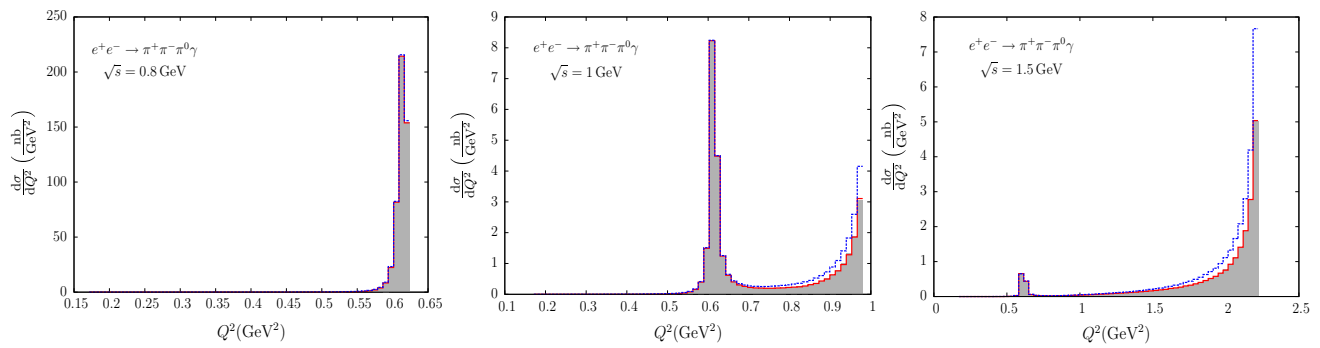
Fig. 13 The differential cross sections of (13) as functions of invariant mass of the $\pi^+\pi^-\pi^0$-system. Legend as in Fig. 11
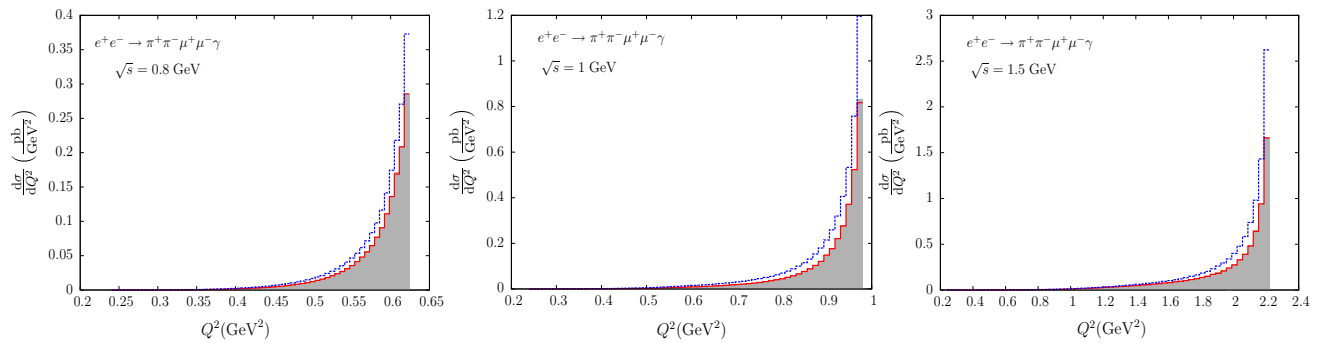

Fig. 14 The differential cross sections of (10) as functions of invariant mass of the $\pi^+\pi^-\mu^+\mu^-$-system. Legend as in Fig. 11
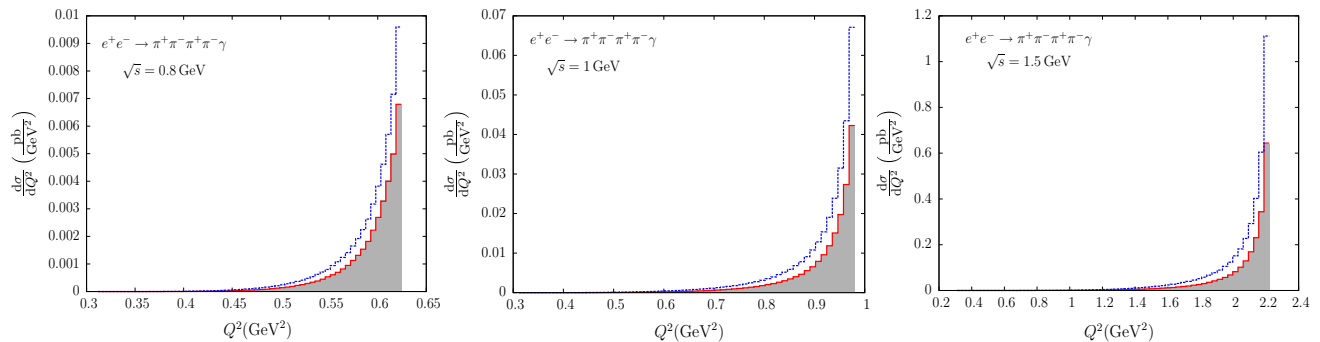

Fig. 15 The differential cross sections of (14) as functions of invariant mass of the $\pi^+\pi^-\pi^+\pi^-$-system. Legend as in Fig. 11

with the corresponding LO cross sections calculated in the HLS model defined by the Feynman rules of Figs. 7, 8 and 9 with fixed couplings. The fixed coupling cross sections receive contribution from 26 Feynman diagrams. They are plotted with dotted lines.

The differential cross sections of processes (13), (10) and (14) corresponding to those plotted in Fig. 11 are shown, respectively, in Figs. 13, 14 and 15 as functions of the invariant mass of the $\pi^+\pi^-\pi^0$-, $\pi^+\pi^-\mu^+\mu^-$-, or $\pi^+\pi^-\pi^+\pi^-$-system. As can be seen in Fig. 15, the FSR effect in the four pion cross section at the c.m.s. energies presented is quite substantial. Although we do not present here the cross sections at energies relevant for the radiative return analysis of that channel at B factories, which would go well beyond the

scope of the present work, we expect that the FSR effects are much smaller relative to the ISR for higher energies, as e.g. the energy of $\Upsilon(4S)$ meson.

In Fig. 16, we make the same comparison for the cross sections of process (10) as was made in Fig. 12 for process (4). This time `carlomat_3.1` generates 627 Feynman diagrams in the HLS model with the fixed couplings.

To illustrate the effect of the FSR in processes with two photons, the ISR (shaded histograms) and full LO (dashed lines) differential cross sections of processes (15), (16) and (17) at $\sqrt{s} = 1$ GeV are plotted in Fig. 17 as functions of invariant mass of the $\pi^+\pi^-$-, $\pi^+\pi^-\mu^+\mu^-$ and $\pi^+\pi^-\pi^+\pi^-$-systems, respectively. We see that this time the FSR effect is much bigger.
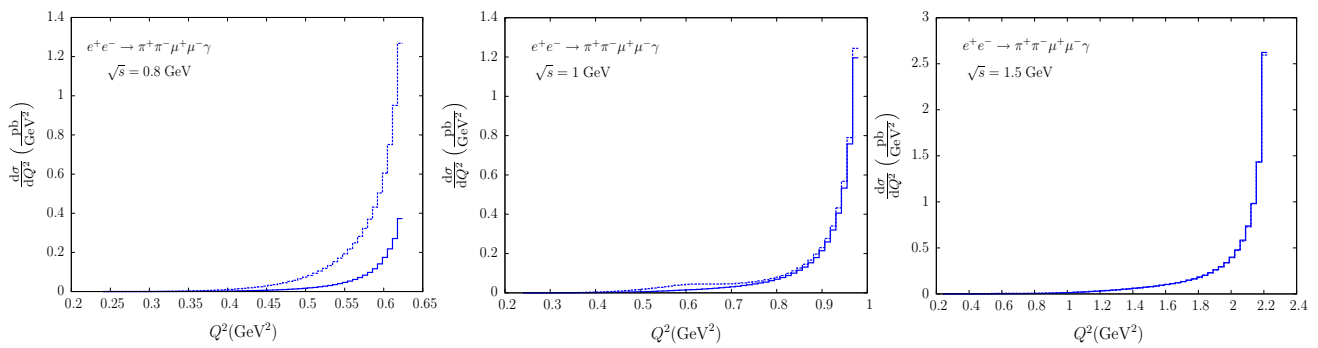
Fig. 16 The differential cross sections of (10) as functions of invariant mass of the $\pi^+\pi^-\mu^+\mu^-$-system computed in a model with the charged pion form factor (*solid lines*) and in the HLS model with fixed couplings (*dotted lines*)
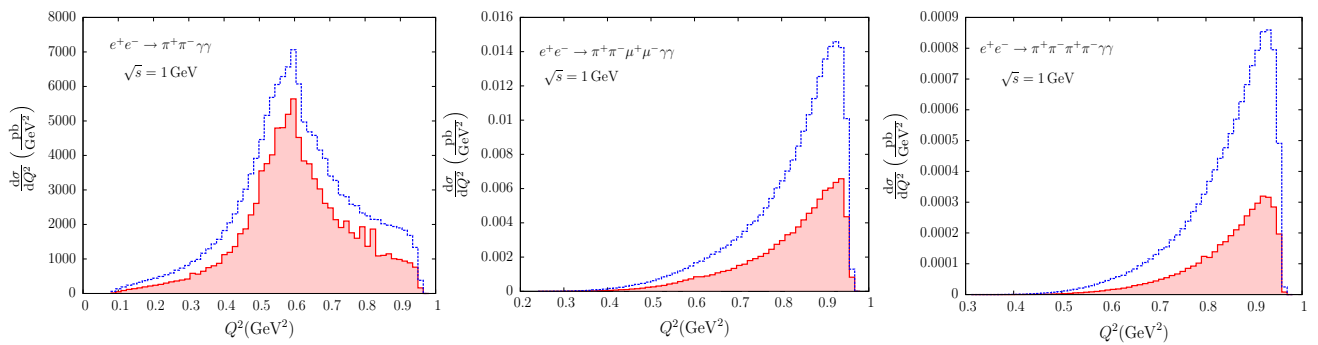

Fig. 17 The differential cross sections of (15), (16) and (17) at $\sqrt{s} = 1$ GeV as functions of invariant mass of the $\pi^+\pi^-$-, $\pi^+\pi^-\mu^+\mu^-$ and $\pi^+\pi^-\pi^+\pi^-$-systems, respectively

4 Summary

We have implemented the electromagnetic charged pion form factor in `carlomat_3.1`, a new version of a multipurpose program `carlomat` that allows one to generate automatically the MC programs dedicated to the description of, among others, the processes $e^+e^- \rightarrow$ hadrons at low centre-of-mass energies. We have illustrated possible applications of the program by considering a photon radiation off the initial and final state particles for a few potentially interesting processes involving charged pion pairs. We have also discussed some problems related to the $U(1)$ electromagnetic gauge invariance that may arise if the momentum transfer dependence is introduced in the couplings of the HLS model or a set of the couplings implemented in the program is incomplete.

References

1. J. Brau, Y. Okada, N. Walker, et al. [ILC collaboration], ILC reference design report: ILC global design effort and world wide study. arXiv:0712.1950 [physics.acc-ph]
2. J.A. Aguilar-Saavedra, et al. [ECFA/DESY LC Physics Working Group Collaboration], TESLA: the superconducting electron positron linear collider with an integrated x-ray laser laboratory. Technical design report. Part 3. Physics at an e^+e^- linear collider. arXiv:hep-ph/0106315
3. T. Abe, et al. [American Linear Collider Working Group collaboration], Linear collider physics resource book for Snowmass 2001—part 2: Higgs and supersymmetry studies. arXiv:hep-ex/0106056
4. K. Abe, et al. [ACFA Linear Collider Working Group collaboration], Particle physics experiments at JLC. arXiv:hep-ph/0109166
5. CLIC Study. http://clic-study.web.cern.ch/clic-study/
6. FCC-ee design study. http://tlep.web.cern.ch/
7. M. Ahmad, et al. [CEPC-SPPC Study Group], CEPC-SPPC preliminary conceptual design report: volume I—physics and detector. http://cepc.ihep.ac.cn/preCDR/volume.html
8. A. Apyan, et al. [CEPC-SPPC Study Group], CEPC-SPPC preliminary conceptual design report: volume II—accelerator. http://cepc.ihep.ac.cn/preCDR/volume.html
9. N. Cabibbo, R. Gatto, Phys. Rev. Lett. **4**, 313 (1960)
10. N. Cabibbo, R. Gatto, Phys. Rev. **124**, 1577 (1961)
11. S. Eidelman, F. Jegerlehner, Z. Phys, C **67**, 585 (1995)
12. R. Alemany, M. Davier, A. Höcker, Eur. Phys. J. C **2**, 123 (1998)

13. J.H. Kühn, M. Steinhauser, Phys. Lett. B **437**, 425 (1998)
14. R.V. Harlander, M. Steinhauser, Comput. Phys. Commun. **153**, 244 (2003)
15. K. Hagiwara, R. Liao, A.D. Martin, D. Nomura, T. Teubner, J. Phys. G G **38**, 085003 (2011)
16. Z. Zhang, EPJ Web Conf. **118**, 01036 (2016). doi:10.1051/epjconf/201611801036
17. M. Davier, A. Höcker, B. Malaescu, Z. Zhang, Adv. Ser. Direct. High Energy Phys. **26**, 129 (2016)
18. F. Jegerlehner, EPJ Web Conf. **118**, 01016 (2016)
19. R.R. Akhmetshin, et al. [CMD-2 Collab.], Phys. Lett. B **578**, 285 (2004). arXiv:hep-ex/0308008
20. V.M. Aulchenko, et al. [CMD-2 Collab.], JETP Lett. **82**, 743 (2005). [Pisma Zh. Eksp. Teor. Fiz. **82**, 841 (2005)]. arXiv:hep-ex/0603021
21. R.R. Akhmetshin, et al., JETP Lett. **84**, 413 (2006). [Pisma Zh. Eksp. Teor. Fiz. **84**, 491 (2006)]. arXiv:hep-ex/0610016
22. R.R. Akhmetshin, et al. [CMD-2 Collab.], Phys. Lett. B **648**, 28 (2007). arXiv:hep-ex/0610021
23. M.N. Achasov, et al. [SND Collab.], J. Exp. Theor. Phys. **103**, 380 (2006). [Zh. Eksp. Teor. Fiz. **130**, 437 (2006)]. arXiv:hep-ex/0605013
24. A. Aloisio, et al. [KLOE Collab.], Phys. Lett. B **606**, 12 (2005). arXiv:hep-ex/0407048
25. F. Ambrosino et al. [KLOE Collab], Phys. Lett. B **670**, 285 (2009). arXiv:0809.3950 [hep-ex]
26. F. Ambrosino et al. [KLOE Collab], Phys. Lett. B **700**, 102 (2011). arXiv:1006.5313 [hep-ex]
27. D. Babusci et al. [KLOE Collab], Phys. Lett. B **720**, 336 (2013). arXiv:1212.4524 [hep-ex]
28. B. Aubert, et al. [BaBar Collab.], Phys. Rev. Lett. **103**, 231801 (2009). arXiv:0908.3589 [hep-ex]
29. J.P. Lees et al. [BaBar Collab], Phys. Rev. D **86**, 032013 (2012). arXiv:1205.2228 [hep-ex]
30. M. Ablikim et al. [BESIII Collab], Phys. Lett. B **753**, 629 (2016). arXiv:1507.08188 [hep-ex]
31. B. Aubert et al. [BABAR Collab], Phys. Rev. D **70**, 072004 (2004)
32. B. Aubert et al. [BABAR Collab], Phys. Rev. D **71**, 052001 (2005)
33. B. Aubert et al. [BABAR Collab], Phys. Rev. D **73**, 012005 (2006)
34. B. Aubert et al. [BABAR Collab], Phys. Rev. D **73**, 052003 (2006)
35. B. Aubert et al. [BABAR Collab], Phys. Rev. D **76**, 012008 (2007)
36. B. Aubert et al. [BABAR Collab], Phys. Rev. D **76**, 092006 (2007)
37. B. Aubert et al. [BABAR Collab], Phys. Rev. D **77**, 092002 (2008)
38. J.P. Lees et al. [BaBar Collab], Phys. Rev. D **85**, 112009 (2012)
39. J.P. Lees et al. [BaBar Collab], Phys. Rev. D **86**, 012008 (2012)
40. J.P. Lees et al. [BaBar Collab], Phys. Rev. D **87**, 092005 (2013)
41. J.P. Lees et al. [BaBar Collab], Phys. Rev. D **88**, 032013 (2013)
42. J.P. Lees et al. [BaBar Collab], Phys. Rev. D **89**, 092002 (2014)
43. J. Lees et al. [BABAR Collab], Phys. Rev. D **87**, 092005 (2013)
44. J. Lees et al. [BABAR Collab], Phys. Rev. D **88**, 032013 (2013)
45. J. Lees et al. [BABAR Collab], Phys. Rev. D **89**, 092002 (2014)
46. M. Davier, Nucl. Part. Phys. Proc. **260**, 102 (2015)
47. R. Akhmetshin et al. [CMD-3 Collab], Phys. Lett. B **723**, 82 (2013)
48. R.R. Akhmetshin et al. [CMD-3 Collaboration], Phys. Lett. B **759**, 634 (2016). doi:10.1016/j.physletb.2016.04.048. arXiv:1507.08013 [hep-ex]
49. E.A. Kozyrev et al. [CMD-3 Collaboration], Phys. Lett. B **760**, 314 (2016). doi:10.1016/j.physletb.2016.07.003. arXiv:1604.02981 [hep-ex]
50. M. Achasov et al., SND Collab. Phys. Rev. D **88**, 054013 (2013)
51. V.M. Aulchenko et al. [SND Collaboration], Phys. Rev. D **91**, 052013 (2015). doi:10.1103/PhysRevD.91.052013. arXiv:1412.1971 [hep-ex]
52. M.N. Achasov et al. [SND Collaboration], Phys. Rev. D **93**, 092001 (2016). doi:10.1103/PhysRevD.93.092001. arXiv:1601.08061 [hep-ex]
53. J.Z. Bai et al. [BES Collab], Phys. Rev. Lett. **84**, 594 (2000)
54. J.Z. Bai et al. [BES Collab], Phys. Rev. Lett. **88**, 101802 (2002)
55. M. Ablikim et al., Phys. Lett. B **677**, 239 (2009)
56. V.V. Anashin et al., Phys. Lett. B **753**, 533 (2016). doi:10.1016/j.physletb.2015.12.059. arXiv:1510.02667 [hep-ex]
57. V.V. Anashin et al., arXiv:1610.02827 [hep-ex]
58. PHOKHARA, http://ific.uv.es/~rodrigo/phokhara/
59. K. Kołodziej, Comput. Phys. Commun. **196**, 563 (2015). arXiv:1504.05915 [hep-ph]
60. M. Benayoun, P. David, L. DelBuono, F. Jegerlehner, Eur. Phys. J. C **73**, 2453 (2013)
61. M. Benayoun, P. David, L. DelBuono, F. Jegerlehner, Eur. Phys. J. C **75**(12), 613 (2015). arXiv:1507.02943 [hep-ph]
62. B. Ananthanarayan, G. Colangelo, J. Gasser, H. Leutwyler, Phys. Rep. **353**, 207 (2001)
63. G. Colangelo, J. Gasser, H. Leutwyler, Nucl. Phys. B **603**, 125 (2001)
64. I. Caprini, G. Colangelo, J. Gasser, H. Leutwyler, Phys. Rev. D **68**, 074006 (2003)
65. B. Ananthanarayan, I. Caprini, G. Colangelo, J. Gasser, H. Leutwyler, Phys. Lett. B **602**, 218 (2004)
66. F. Jegerlehner, R. Szafron, Eur. Phys. J. C **71**, 1632 (2011)
67. J. Gluza, A. Hoefer, S. Jadach, F. Jegerlehner, Eur. Phys. J. C **28**, 261 (2003)
68. G. Pancheri, O. Shekhovtsova, G. Venanzoni, Phys. Lett. B **642**, 342 (2006)
69. F. Ambrosino et al. [KLOE Collab], Phys. Lett. B **634**, 148 (2006)
70. F. Ambrosino et al. [KLOE Collab], Eur. Phys. J. C **49**, 473 (2007)
71. H. Marsiske et al. [Crystal Ball Collab], Phys. Rev. D **41**, 3324 (1990)
72. J.K. Bienlein, DESY-92-083B
73. T. Oest et al. [JADE Collab], Z. Phys. C **47**, 343 (1990)
74. J. Boyer et al. [for the MARK II Collab], Phys. Rev. D **42**, 1350 (1990)
75. C. Berger et al. [PLUTO Collab], Z. Phys. C **26**, 199 (1984)
76. H.J. Behrend et al. [CELLO Collab], Z. Phys. C **56**, 381 (1992)
77. H. Nakazawa et al. [BELLE Collab], Phys. Lett. B **615**, 39 (2005)
78. S. Uehara et al., Phys. Rev. D **79**, 052009 (2009)
79. S. Uehara et al., Phys. Rev. D **78**, 052004 (2008)
80. M. Masuda et al. [Belle Collaboration], Phys. Rev. D **93**, 032003 (2016)
81. K. Kołodziej, carlomat_3.1 a current version of the program dedicated to the description of processes of electron-positron annihilation to hadrons at low centre of mass energies. http://kk.us.edu.pl/carlomat.html
82. S. Binner, Johann H. Kühn, K. Melnikov, Phys. Lett. B **459**, 279 (1999). arXiv:hep-ph/9902399
83. K. Kołodziej, Comput. Phys. Commun. **180**, 1671 (2009). arXiv:0903.3334 [hep-ph]